JOURNAL OF AIRCRAFT
Vol. 45, No. 5, September–October 2008

Flexible-Membrane Airfoils at Low Reynolds Numbers

Hui Hu,* Masatoshi Tamai,† and Jeffery T. Murphy†
Iowa State University, Ames, Iowa 50011

DOI: 10.2514/1.36438

An experimental study was conducted to assess the benefits of using flexible-membrane airfoils/wings at low Reynolds numbers for micro air vehicle applications compared with using a conventional rigid airfoil/wing. In addition to measuring aerodynamic forces acting on flexible-membrane airfoils/wings, a high-resolution particle image velocimetry system was used to conduct flowfield measurements to quantify the transient behavior of vortex and turbulent flow structures around the flexible-membrane airfoils/wings to elucidate the associated underlying fundamental physics. The aerodynamic force measurements revealed that flexible-membrane airfoils could provide better aerodynamic performance compared with their rigid counterpart at low Reynolds numbers. The flexibility (or rigidity) of the membrane skins of the airfoils was found to greatly affect their aerodynamic performance. Particle image velocimetry measurements elucidated that flexible-membrane airfoils could change their camber (i.e., cross-sectional shape) automatically to adapt incoming flows to balance the pressure differences on the upper and lower surfaces of the airfoils, therefore suppressing flow separation on the airfoil upper surfaces. Meanwhile, deformation of the flexible-membrane skins was found to cause significant airfoil trailing-edge deflection (i.e., lift the airfoil trailing edge up from its original designed position), which resulted in a reduction of the effective angles of attack of the flexible-membrane airfoils, thereby delaying airfoil stall at high angles of attack. The nonuniform spanwise deformation of the flexible-membrane skins of the flexible-membrane airfoils was found to significantly affect the characteristics of vortex and turbulent flow structures around the flexible-membrane airfoils.

Nomenclature

C	=	chord length of the airfoil
C_l, C_d	=	lift-and-drag coefficients
N	=	total number of frames of the instantaneous PIV measurements
Re_C	=	chord Reynolds number
U	=	mean velocity components in the x direction, $\Sigma_{i=1}^{N} u_i/N$
u_i, v_i	=	instantaneous velocity components in the x and y directions
V	=	mean velocity components in the y direction, $\Sigma_{i=1}^{N} v_i/N$
V_∞	=	incoming flow velocity
x, y	=	Cartesian coordinate directions
ω_z	=	spanwise vorticity, $(\partial v_i/\partial x) - (\partial u_i/\partial y)$

Introduction

MICRO air vehicles (MAVs), which are characterized by small vehicle size (approximately 10 cm) and low flight speeds (approximately 10 m/s), are of great interest to both military and civilian applications. Equipped with video cameras, transmitters, or sensors, these miniaturized aerial vehicles can perform surveillance, reconnaissance, targeting, or biochemical sensing tasks at remote, hazardous, or dangerous locations. Research progress made in recent years has resulted in advances in miniaturized digital electronics, microfabrication, miniaturized power cells, remote communication, imaging and control devices, and other enabling technologies. Such advances have turned the concept of MAVs as rapidly deployable eyes-in-the-sky from fiction into demonstrated fact. The continuing demand for such small and robust miniaturized aerial vehicles is making MAVs an emerging sector of the aerospace market.

Although a number of MAVs, either in fixed-wing or flapping-wing designs, have already been developed by universities and commercial- and government-funded endeavors, the airfoil and wing planform designs for many existing MAVs rely mainly on scaled-down reproductions of those used by conventional macroscale aircraft. Chord Reynolds number Re_C, which is based on airfoil chord length and flight velocity, is usually used to characterize the aerodynamic performance of an airfoil/wing. Although traditional macroscale aircraft have a chord Reynolds number of about 10^6–10^8, the low flight speed and miniaturized size of MAVs make their chord Reynolds numbers typically in the range of 10^4–10^5. The aerodynamic design principles applicable to traditional macroscale aircraft may not be used for MAVs, due to the significant difference in chord Reynolds numbers [1,2]. As a result, airfoil shape and wing planform designs that are optimized for traditional macroscale aircraft are found to degrade significantly when used for miniaturized aircraft such as MAVs [3,4]. Therefore, it is very necessary and important to establish novel airfoil shape and wing planform design paradigms for MAVs to achieve acceptable aerodynamic performance as well as flight agility and versatility.

Thin and flexible-membrane wings are unique to flying and gliding mammals, such as bats, flying squirrels, and sugar gliders. These animals exhibit extraordinary flight capabilities with respect to maneuvering and agility that are not observed in other species of comparable size. Birds, which have been studied extensively, have relatively rigid wings with limited motion, whereas insects, which fly at much lower Reynolds numbers, are typically characterized by rigid wings moving with a relatively simply articulated flapping motion. Bats, on the other hand, have an extremely high degree of articulation in the wing (the elbow, wrist, and finger joints). More relevant to the present study is the fact that the wing surface in bats is composed of a thin flexible membrane [5–8]. This observation suggests that a potentially useful feature for engineered maneuverable MAVs might be the incorporation of flexible membranes as lifting surfaces. With this in mind, we conducted the present study to try to leverage the unique feature of flexible-membrane airfoils/wings found in bats and other flying/gliding mammals to explore the potential applications of such nontraditional bioinspired flexible-membrane airfoils/wings to MAV designs for improved aerodynamic performance.

Received 2 January 2008; accepted for publication 28 April 2008.

*Assistant Professor, Aerospace Engineering Department; huhui@iastate.edu. Senior Member AIAA.
†Graduate Student, Aerospace Engineering Department.

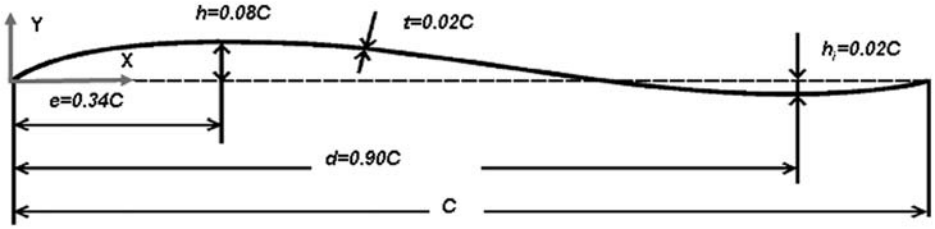

Fig. 1 Cross section of the test airfoils.

It should be noted that the MAV team of the University of Florida (UF), who have achieved great success in international MAV competitions in the past several years, is the first team to adopt flexible-membrane airfoil/wing design to build UF flexible-wing-based MAVs. The flexible-wing-based MAVs developed by the UF-MAV research group [9–13] consists of a leading-edge spar and chordwise battens that are made of unidirectional carbon fiber. Membrane material is bonded to the spar and battens to be the skin of the airfoils/wings. In a turbulent atmosphere that is typical for low Reynolds number flight, the flexible-membrane-wing-based structures were found to be able to absorb the inconsistencies in the air currents, thereby providing improved stability to the vehicle as a whole. This technology, called gust suppression or adaptive washout, has been regarded as the key element for the UF-MAV team's success in winning the international MAV competitions for the past several years [13].

It is fair to say that flexible-membrane airfoils/wings have received only a small fraction of the technological attention that has been given to rigid airfoils/wings. Although flexible-membrane airfoils/wings have been suggested to be able to alleviate the effects of gust wind, delay airfoil stall, and provide additional advantages for morphing to achieve enhanced agility and storage compared with rigid airfoils/wings for MAV applications [9–19], the fundamental physics associated with why and how flexible-membrane airfoils/wings could provide advantages in gust alleviation and stall suppression is still not well understood. The majority of previous experimental studies on flexible-membrane airfoils/wings were conducted based mainly on measuring overall aerodynamic forces and/or moments acting on the flexible-membrane airfoils/wings [10,13,18,19], and very little in literature can be found related to the transient behavior of unsteady vortex and turbulent flow structures around flexible-membrane skins as well as their effects on the overall aerodynamic performance of the flexible-membrane airfoils/wings.

In the present study, an experimental study was conducted to investigate the benefits of using flexible-membrane airfoils/wings at low Reynolds numbers for MAV applications compared with a conventional rigid airfoil/wing. By adding different numbers of rigid ribs to the same membrane-airfoil configuration to adjust the flexibility of the membrane skins of the airfoils, the effects of the flexibility (or rigidity) of the membrane airfoils on their aerodynamic performance were also assessed in the present study. In addition to measuring aerodynamic forces acting on the flexible-membrane airfoils/wings, a high-resolution particle image velocimetry (PIV) system was used to conduct quantitative flowfield measurements to visualize the transient behavior of vortex and turbulent flow structures around the flexible-membrane airfoils/wings at different angles of attack (AOA). The flowfield measurements were correlated with the total aerodynamic force measurements to elucidate underlying fundamental physics to explore/optimize design paradigms for the development of novel bioinspired flexible-membrane-wing-based MAVs for improved aerodynamic performance.

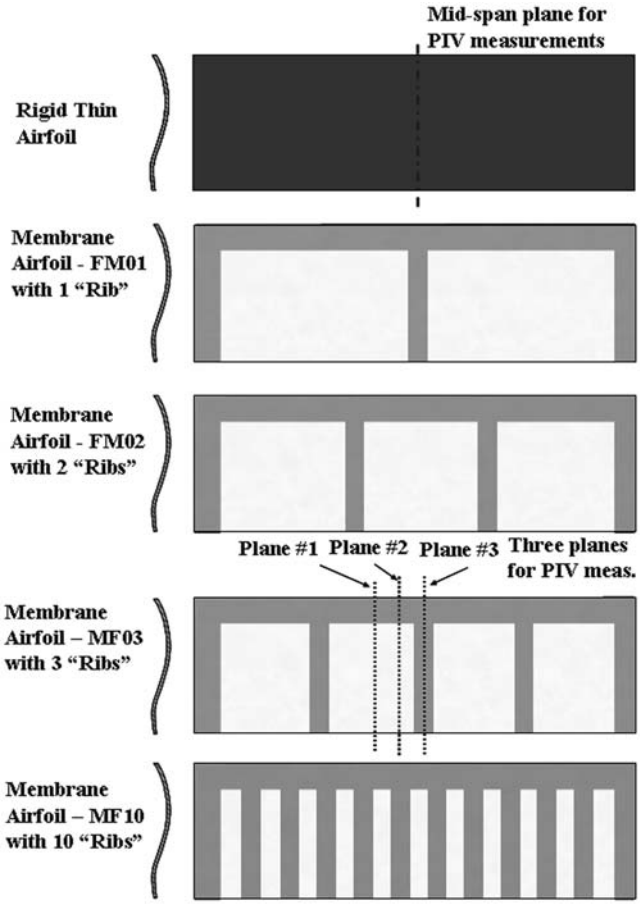

Fig. 2 Test airfoils and the locations of the cross planes for PIV measurements.

Studied Airfoils and Experimental Setup

The experimental study was performed in a closed-circuit low-speed wind tunnel located in the Aerospace Engineering Department of Iowa State University. The tunnel has a test section with a 1.0 by 1.0 ft (30 by 30 cm) cross section and optically transparent walls. The tunnel has a contraction section upstream of the test section with

Table 1 The design parameters of the studied airfoils

Studied airfoil	Numbers of ribs	Spanwise length of each latex skin, mm	Percentage of flexible surface, %	Percentage of rigid surface, %
Rigid airfoil	None	None	0	100
FM01	1	127.0	83.9	16.1
FM02	2	82.6	80.2	19.8
FM03	3	60.3	74.7	25.3
FM10	10	18.5	59.2	40.8

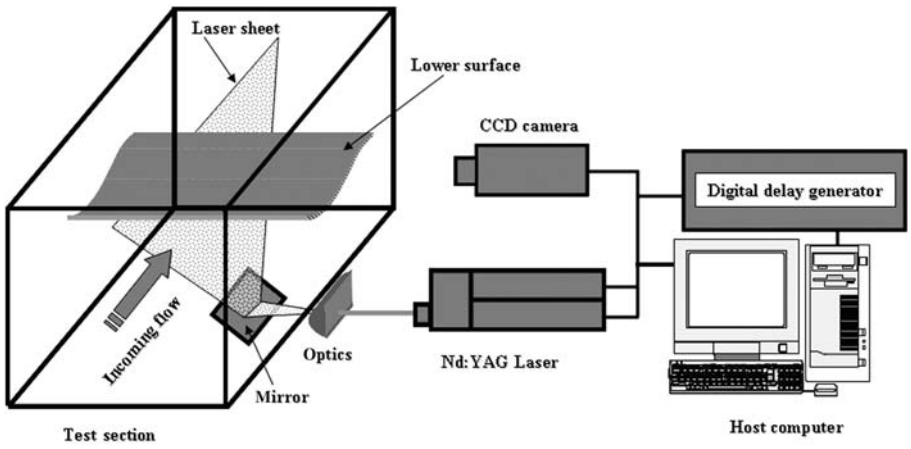

Fig. 3 Experimental setup.

screen structures and a cooling system installed ahead of the contraction section to provide uniform low-turbulent incoming flow to enter the test section.

All the airfoils used in the present study have the same cross-sectional shape and chord length of 105 mm (i.e., $C = 105$ mm). As shown in Fig. 1, the airfoil cross-sectional shape design is similar to that used by Null and Shkarayev [20]. One unique feature of the airfoil is that there exists a small inverse camber section at the rear portion of the airfoils to compensate for the high positive pitching moment for MAV applications. Such thin cambered airfoil shape design has already been used widely by several research groups to successfully make functional MAVs.

Figure 2 shows the five airfoils studied in the present study: a rigid airfoil as the comparison baseline and four flexible-membrane airfoils with different numbers of rigid ribs to adjust the flexibility of the membrane skins of the membrane airfoils. The rigid airfoil is made of unidirectional carbon fiber with the thickness of 1.15 mm. As shown in Fig. 2, the flexible-membrane airfoils have the same rigid main frames (leading-edge spar and two side battens), which were made of unidirectional carbon fiber. Flexible-membrane material (latex sheet) is wrapped around the airfoil main frames at both the upper and lower airfoil surfaces. Although the membrane skins are flexible and do not sustain a bending moment, the carbon-fiber main frames and ribs are rigid and can therefore sustain bending moment as well as provide structural support. Table 1 gives the design parameters of the studied airfoils. Further information about the geometry design and manufacturing process of the rigid- and flexible-membrane airfoils is available in [21].

In the present study, the velocity of the incoming flow was set as $U_\infty = 11.0$ m/s, which corresponds to a chord Reynolds number of $Re_C = 70,000$. The turbulence intensity of the incoming flow was found to be about 0.8%, measured by using a hot-wire anemometer.

Figure 3 shows the experimental setup used in the present study for PIV measurements. During the experiment, the test airfoils were installed in the middle of the test section. A PIV system was used to make flow-velocity field measurements around the airfoils. The spanwise locations of the cross planes for the PIV measurements is shown in Fig. 2. The flow was seeded with 1–5-μm oil droplets. Illumination was provided by a double-pulsed Nd:YAG laser (NewWave Gemini 200) emitting two pulses of 200 mJ at the wavelength of 532 nm with a repetition rate of 10 Hz. The laser beam was shaped to a laser sheet (thickness $\sim$1 mm) by using a set of mirrors and spherical and cylindrical lenses. A high-resolution 12-bit (1376×1040 pixels) charge-coupled device (CCD) camera (SensiCam-QE, Cooke Corp.) was used for PIV image acquisition, with its axis perpendicular to the laser sheet. The CCD camera and the double-pulsed Nd:YAG lasers were connected to a workstation via a digital delay generator, which controlled the timing of the laser illumination and the image acquisition.

Instantaneous PIV velocity vectors were obtained by a frame-to-frame cross-correlation technique involving successive frames of patterns of particle images in an interrogation window of

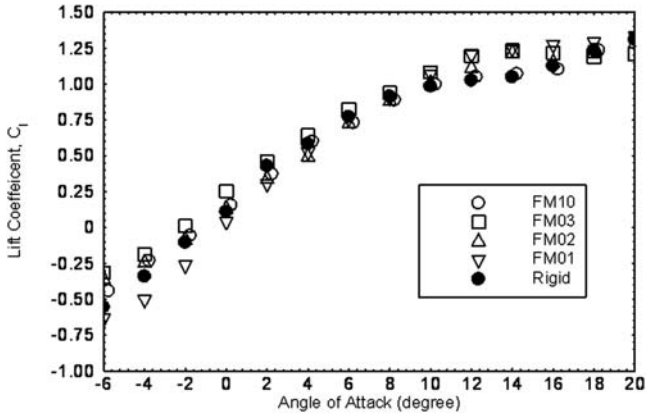

a) Lift coefficient vs angle of attack

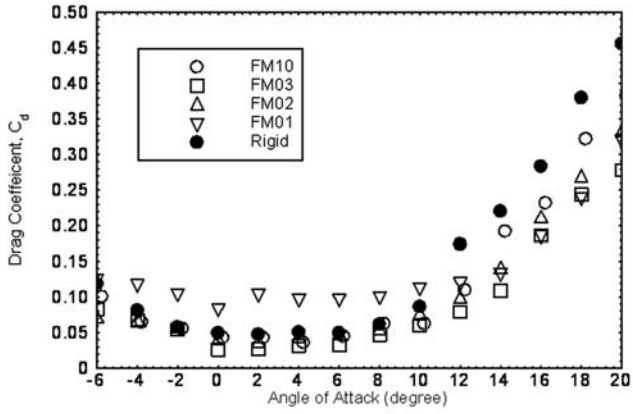

b) Drag coefficient vs angle of attack

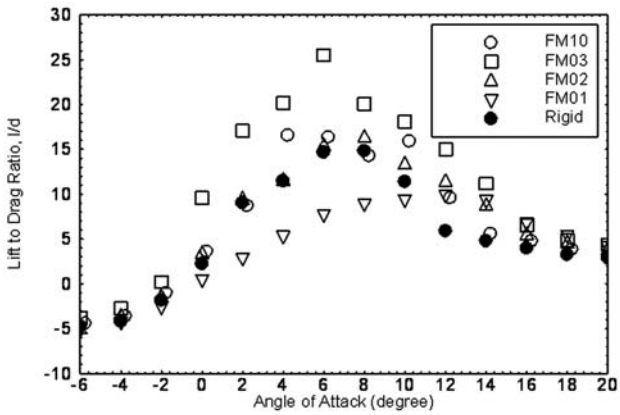

c) Lift to drag ratio vs angle of attack

Fig. 4 Measured lift-and-drag coefficients.

32×32 pixels. An effective overlap of 50% was employed for the PIV image processing. After the instantaneous velocity vectors u_i and v_i were determined, the spanwise vorticity ω_z could be derived. Ensemble-averaged velocity (U, V) was obtained from a cinema sequence of 400 frames of instantaneous velocity fields. The measurement uncertainty level for the PIV measurements is estimated to be within 2%.

The aerodynamic forces (lift and drag) acting on the test airfoils were measured by using a force-moment sensor cell (JR3, model 30E12A-I40). The force-moment sensor cell is composed of foil strain-gauge bridges, which are capable of measuring the forces on three orthogonal axes and the moment (torque) about each axis. The precision of the force-moment sensor cell for force measurements is $\pm 0.25\%$ of the full scale (40 N).

Experimental Results and Discussions

Aerodynamic Force Measurement Results

Figure 4 shows the measurement results of the aerodynamic forces acting on the studied airfoils in the terms of lift coefficient and drag coefficient as the AOA of the airfoils changed from -6.0 to 20.0 deg.

For the rigid thin airfoil, whereas the lift coefficient was found to increase almost linearly with the increasing AOA, as expected, the drag coefficient was reasonably small when the angle of attack was relatively low (AOA < 10.0 deg). The increase rate of the lift coefficient was found to flatten out at relatively high angles of attack. The drag coefficient of the rigid thin airfoil was found to increase significantly at AOA > 10.0 deg. Such characteristics revealed in the lift- and drag-coefficient profiles indicates that airfoil stall occurred for the rigid thin airfoil at AOA > 10.0 deg, which was visualized clearly from the PIV measurements to be discussed later.

The flexible-membrane airfoils FM02, FM03, and FM10 were found to have very comparable or a slightly larger lift coefficient than the rigid thin airfoil. The drag coefficient of the flexible-membrane airfoils was found to be significantly smaller than that of the rigid thin airfoil at relatively high angles of attack (AOA > 10.0 deg). Airfoil stall (i.e., a flattened increase rate of lift coefficient and dramatic increase of drag coefficient) was found to occur at higher angles of attack for the flexible-membrane airfoils than for the rigid thin airfoil. Such measurement results confirmed the fact that flexible-membrane airfoils could delay airfoil stall, as suggested by previous studies [22].

It should be noted that the flexible-membrane airfoil FM01, which has only one rigid rib placed in the middle of the two rigid side battens (Fig. 2), is the most flexible airfoil among all the tested airfoils. During the experiments, the trailing edge of the flexible-membrane airfoil FM01 was found to be fluttering when the angle of attack was relatively low (AOA < 10.0 deg). As a result, the flexible-membrane airfoil FM01 was found to have the worst aerodynamic performance (i.e., the smallest lift coefficient and largest drag coefficient) among all the tested airfoils at relatively low angles of attack (AOA < 10.0 deg). The trailing-edge fluttering phenomena were found to disappear for the FM01 airfoil when the membrane skins were stretched severely at relatively high angles of

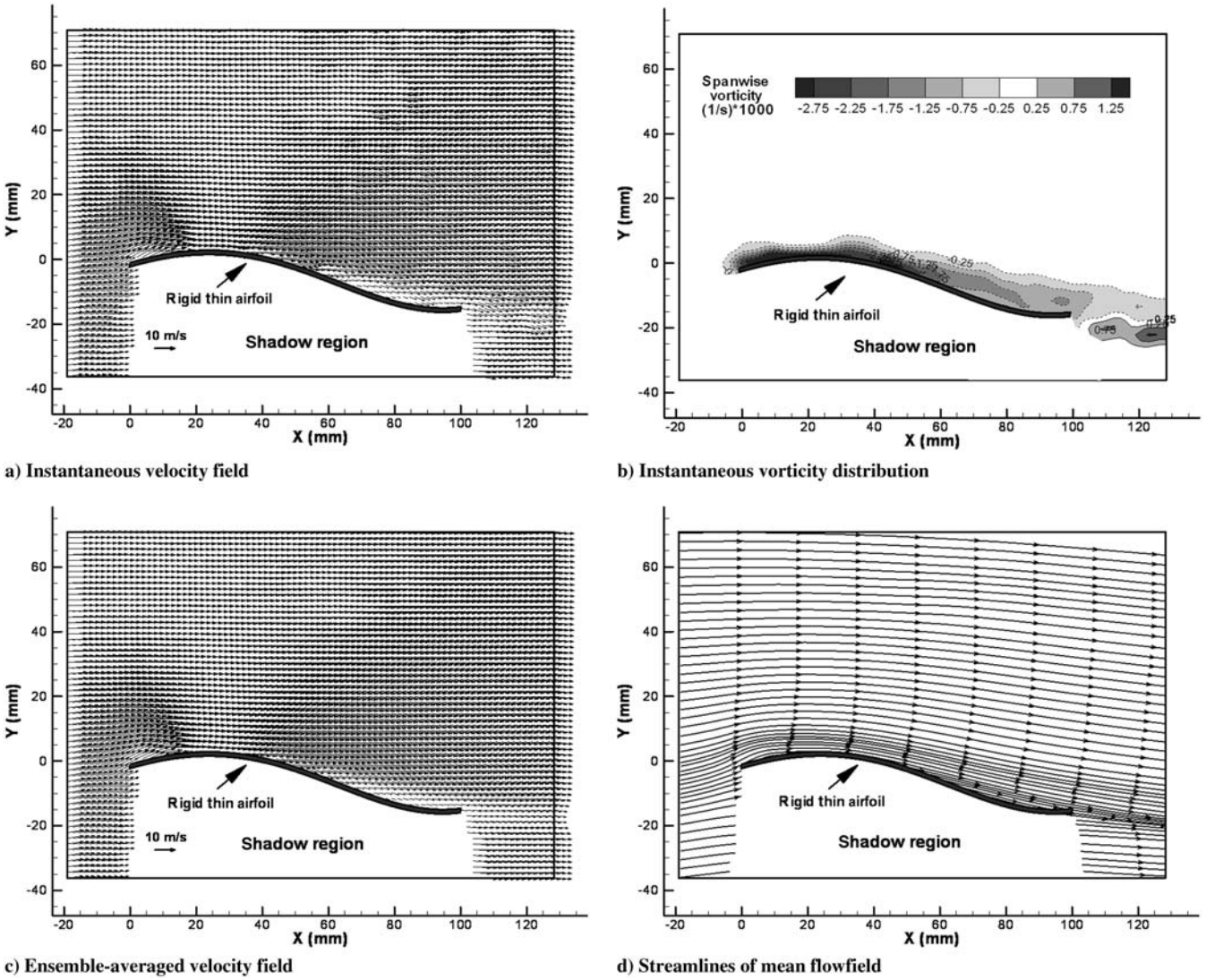

Fig. 5 PIV measurements in the midspan plane of the rigid thin airfoil at AOA = 6.0 deg.

attack. Surprisingly, the FM01 airfoil was found to have almost the best aerodynamic performance (i.e., small drag coefficient and high lift coefficient) among all the tested airfoils when the trailing-edge fluttering phenomena disappeared at the relatively high angle of attack (i.e., AOA $>$ 10.0 deg).

As expected, the flexible-membrane airfoil FM10, which has 10 rigid ribs between the two side battens (and thus the least flexibility among the tested flexible-membrane airfoils) was found to have an aerodynamic performance very similar to the rigid thin airfoil. The flexible-membrane airfoil FM03 was found to have the best aerodynamic performance (e.g., largest lift coefficient and smallest drag coefficient) among all the test airfoils, with the lift-to-drag ratio being up to 25.5 at AOA $=$ 6.0 deg.

The aerodynamic force measurement results revealed that the flexibility (or rigidity) of the membrane skins could significantly affect the aerodynamic performance of the membrane airfoils. Therefore, it is important to chose a proper flexibility (or rigidity) of the membrane skins to achieve improved aerodynamic performance by using flexible-membrane airfoils at low Reynolds numbers for MAV applications.

PIV Measurement Results

With the findings derived from the aerodynamic force measurements in mind, PIV measurements were carried out to visualize the transient behavior of vortex and turbulent flow structures around the flexible-membrane airfoils compared with those around the rigid airfoil to reveal the underlying fundamental physics associated with the airfoil aerodynamic performance characteristics revealed from the aerodynamic force measurements.

Figure 5 shows the PIV measurement results of the flowfield around the rigid thin airfoil at AOA $=$ 6.0 deg. As indicated in Fig. 2, the PIV measurement was conducted in the midspan for the rigid airfoil. Because the adverse pressure gradient over the upper surface of the rigid airfoil was rather mild at AOA $=$ 6.0 deg, the instantaneous and ensemble-averaged measurement results revealed clearly that incoming streams could follow the curved upper surface of the rigid airfoil. A boundary layer was visualized clearly in the instantaneous vorticity distribution as a thin vortex layer affixing to the airfoil upper surface. The boundary layer was found to attach to the airfoil upper surface from the leading edge all the way to the trailing edge. The streamlines of the mean flowfield shows clearly that because the incoming flow streams could flow smoothly to follow the curved surface of the rigid thin airfoil at AOA $=$ 6.0 deg, they left the airfoil trailing edge smoothly, which resulted in a very small wake region (i.e., the region with velocity deficits) downstream of the airfoil. The small wake region downstream of the airfoil indicated a small aerodynamic drag force acting on the airfoil, which was confirmed from the aerodynamic force measurements given in Fig. 4.

The results of the PIV measurements conducted in the midspan cross plane of the rigid thin airfoil at AOA $=$ 10.0 deg are shown in Fig. 6. The adverse pressure gradient over the upper surface of the airfoil became more and more severe as the angle of attack increased.

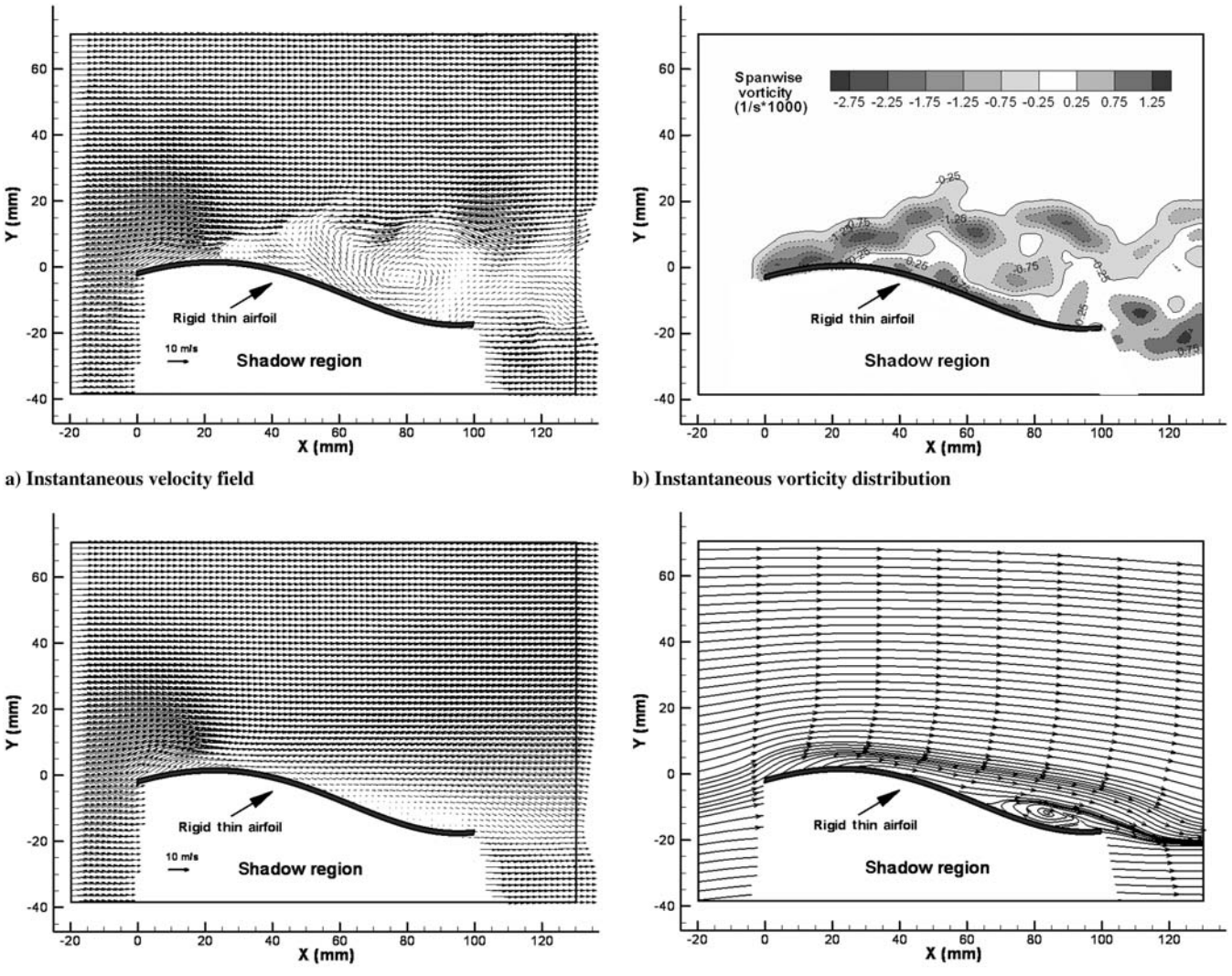

Fig. 6 PIV measurements in the midspan plane of the rigid thin airfoil at AOA = 10.0 deg.

The instantaneous PIV measurement results show clearly that incoming flow streams could not flow smoothly to follow the curved upper surface of the rigid thin airfoil anymore, due to more severe adverse pressure gradient at AOA = 10.0 deg. The boundary-layer flow (i.e, the vortex layer attached to the airfoil surface near the airfoil leading edge) was found to separate from the airfoil upper surface of the airfoil. Strong, unsteady vortex structures were found to be generated in the wake of the rigid thin airfoil as a result of the boundary-layer flow separation. The flow separation on the upper surface of the airfoil can also be seen clearly from the ensemble-averaged PIV measurement results in the form of a separation bubble near the trailing edge of the airfoil. Because of the flow separation, the size of the wake region (i.e. the region with velocity deficits) downstream of the rigid thin airfoil was found to be increased greatly, which indicates an increased aerodynamic drag force acting on the airfoil. The increased aerodynamic drag acting on the rigid thin airfoil at AOA = 10.0 deg was confirmed quantitatively for the measured drag-coefficient data given in Fig. 4.

Figure 7 gives the PIV measurement results of the flowfield around the rigid thin airfoil as the angle of attack increased to 14.0 deg (i.e., AOA = 14.0 deg). The significant adverse pressure gradient over the upper surface of the airfoil at AOA = 14.0 deg caused incoming flow streams to separate from the airfoil upper surface almost from the leading edge of the airfoil; that is, the separation point of the boundary-layer flow was pushed upstream approaching the airfoil leading edge, due to the significant adverse pressure gradient. Large-scale flow separation was found to take place on almost the entire upper surface of the rigid thin airfoil. Very strong, unsteady vortex structures were found to be generated in the wake of the rigid airfoil. As a result, a very large recirculation bubble was found to be formed in the wake of the rigid thin airfoil, which indicates that the airfoil was in a deep-stall state. As revealed quantitatively from the aerodynamic force measurement data given in Fig. 4, the aerodynamic performance of the airfoil was found to degrade significantly, with the drag coefficient of the airfoil increasing dramatically at AOA = 14.0 deg.

Although the flexible-membrane airfoils were designed to have the same cross-sectional shape as the rigid thin airfoil, flexible-membrane skins allow the flexible-membrane airfoils to be able to adjust their cross-sectional shape automatically to adapt to incoming flows to balance the pressure differences on the upper and lower surfaces of the flexible-membrane airfoils at different angles of attack. As shown in Fig. 2, PIV measurements were conducted in three different cross planes along the spanwise direction for the flexible-membrane airfoil FM03. Measurement plane 1 is located in the middle plane between the first and second rigid ribs for the MF03 airfoil, where the membrane skin of the airfoil was found to be the most flexible, and maximum deformation of the cross-sectional shape was observed during the experiments. Measurement plane 3 was selected to be in the center plane of the second rigid rib, which is also the midspan of the FM03 airfoil. Because the rib is rigid, the

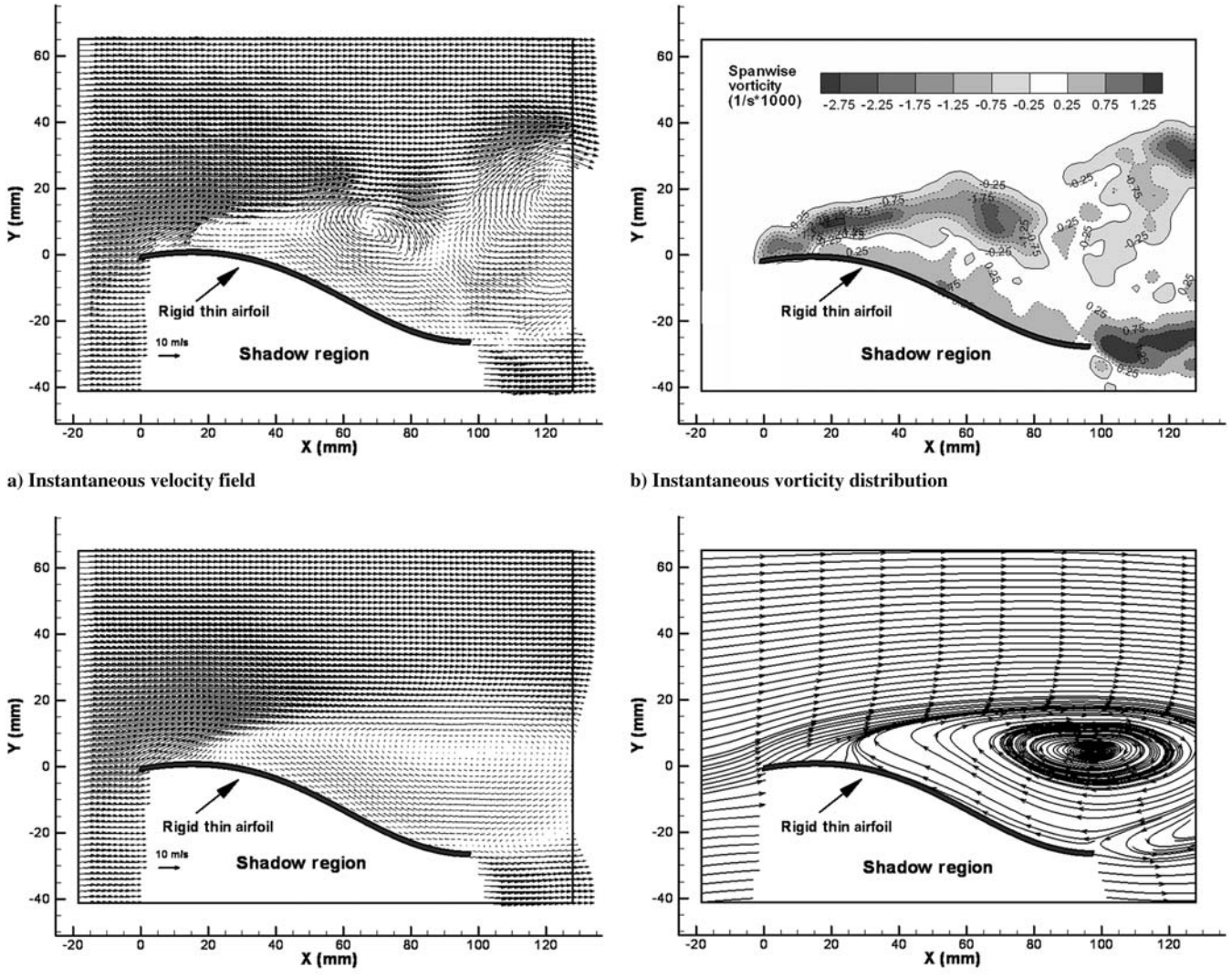

a) Instantaneous velocity field

b) Instantaneous vorticity distribution

c) Ensemble-averaged velocity field

d) Streamlines of mean flowfield

Fig. 7 PIV measurements in the midspan plane of the rigid thin airfoil at AOA = 14.0 deg.

cross-sectional shape of the airfoil in measurement plane 3 would not be deformed during the experiments. Measurement plane 2 was selected to be in the middle plane between measurement plane 1 and measurement plane 3, where the cross section of the airfoil was found to deform during the experiments. However, the deformation amplitude in measurement plane 2 was found to be much more moderate than that in measurement plane 1.

The PIV measurement results of the vortex and turbulent flow structures around the FM03 airfoil in the three measurement planes at different angles of attack are given in Figs. 8–12. The bold dashed lines in the figures indicate the original cross-sectional shape (i.e., designed shape without any deformation) of the FM03 airfoil, and the bold solid lines indicate the actual cross-sectional shapes of the FM03 airfoil in the measurement planes extracted from PIV raw images.

For the rigid thin airfoil, as revealed in the PIV measurement results given in Fig. 6, incoming flow streams were found to separate from the upper surface of the rigid thin airfoil due to a severe adverse pressure gradient at AOA = 10.0 deg. As visualized clearly from the PIV measurement results given in Fig. 8, because the flexible-membrane airfoil FM03 could change its chamber shape (i.e., the shape of the cross section) automatically to adapt incoming flow streams to balance the pressure differences on the upper and lower surfaces of the airfoil, incoming flow streams were found to stay firmly attached to the deformed membrane skin in measurement plane 1 from the airfoil leading edge all the way down to the airfoil trailing edge at AOA = 10.0 deg. No large-scale flow separation was found on the upper surface of the FM03 airfoil in measurement plane 1. Both the instantaneous and ensemble-averaged PIV measurement results revealed clearly that the wake region (i.e., the region with velocity deficits) downstream of the FM03 airfoil in measurement plane 1 is quite small because incoming flow streams can stay attached to the deformed airfoil upper surface at AOA = 10.0 deg. The small wake region indicates a small aerodynamic drag force acting on the FM03 airfoil, which was confirmed from the aerodynamic drag force measurements given in Fig. 4.

As visualized clearly from the PIV measurement results given in Fig. 7, the rigid thin airfoil was found to stall completely at AOA = 14.0 deg due to the significant adverse pressure gradient on the upper surface of the airfoil. Figures 9–11 show the PIV measurement results of the flow structures around the FM03 airfoil at AOA = 14.0 deg in measurement planes 1, 2, and 3, respectively.

From the PIV measurement results shown in Fig. 9, it can be seen clearly that the deformation to the cross-sectional shape of the FM03 airfoil in measurement plane 1 became more severe at AOA = 14.0 deg than those at smaller angles of attack (such as the case of AOA = 10.0 deg, shown in Fig. 8). In addition to changing airfoil cross-sectional shape more severely to balance the pressure differences on the upper and lower surfaces of the airfoil at AOA = 14.0 deg, significant airfoil trailing-edge defection (i.e., to lift the airfoil trailing edge up from its original position) was also found for the FM03 airfoil in measurement plane 1, due to the more severe pressure difference at AOA = 14.0 deg, which resulted in a considerable reduction of the effective angle of attack in measurement plane 1. Because of the deformed cross-sectional

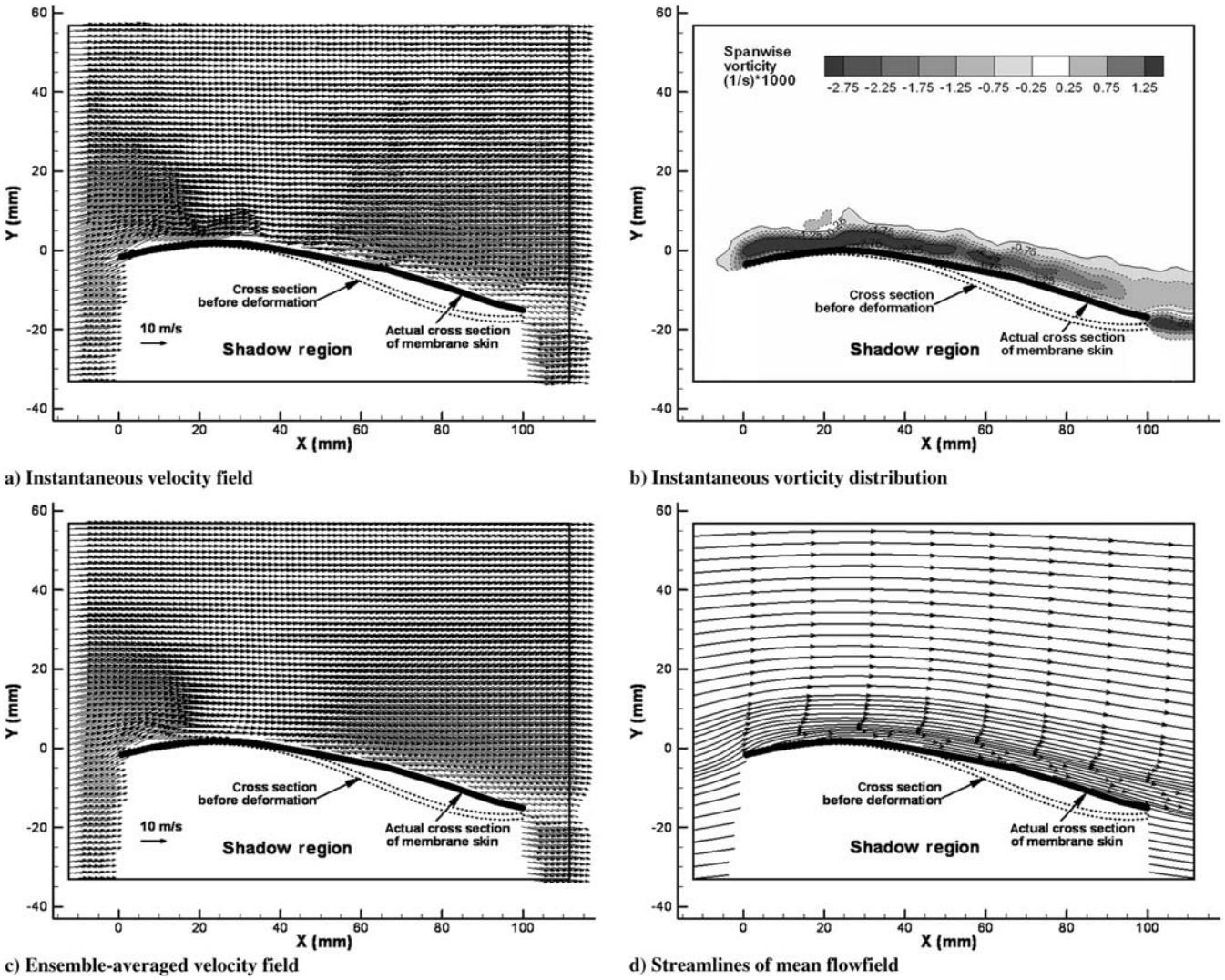

Fig. 8 PIV measurements in measurement plane 1 for the FM03 airfoil at AOA = 10.0 deg.

shape and the effective-angle-of-attack reduction, incoming flow streams were found to be able to stay attached to the deformed airfoil surface in measurement plane 1 for the FM03 airfoil at AOA = 14.0 deg. As a result, the wake region downstream of the FM03 airfoil was found to be still reasonably small in measurement plane 1, whereas a very big recirculation bubble was already found to form downstream of the rigid airfoil at the same angle of attack of AOA = 14.0 deg. Compared with those at smaller angles of attack (such as the case shown in Fig. 8 with AOA = 10.0 deg), the size of the wake region in measurement plane 1 was found to become slightly larger, indicating an increased aerodynamic drag force acting on the airfoil, which is confirmed from the measured airfoil drag coefficient given in Fig. 4.

As shown in Fig. 10, the deformation of the cross-sectional profile of the FM03 airfoil in measurement plane 2 was found to be much more moderate than that in measurement plane 1 at the same angle of attack of AOA = 14.0 deg. Instead of having incoming flow streams attached to the deformed airfoil upper surface from the leading edge to the trailing edge as with those in measurement plane 1 shown in Fig. 9, a time sequence of the instantaneous PIV measurement results in measurement plane 2 revealed that incoming streams would separate from the airfoil upper surface at the rear portion of the airfoil from time to time, accompanied by shedding of unsteady vortex structures in the wake of the airfoil. The ensemble-averaged velocity and corresponding streamline distributions reveal that, whereas incoming flow streams were found to follow the front portion of the deformed profile at the airfoil cross section in measurement plane 2, flow separation near the airfoil trailing edge can be seen clearly from the ensemble-averaged PIV measurement results. As a result, a larger wake region with velocity deficits was found downstream of the FM03 airfoil in measurement plane 2 than that in measurement plane 1 for the FM03 airfoil at the same angle of attack of AOA = 14.0 deg.

Figure 11 shows the PIV measurement results in measurement plane 3 for the FM03 airfoil at AOA = 14.0 deg. As already described, because the ribs of the FM03 airfoil are rigid, the cross-sectional shape of the airfoil would not be changed in measurement plane 3 during the experiments. The incoming flow streams were found to separate from the airfoil upper surface from a location very close to the airfoil leading edge in measurement plane 3. Large-scale flow separation was found to take place on almost the entire upper surface of the airfoil, which results in a very large recirculation region formed downstream of the FM03 airfoil in measurement plane 3, as visualized clearly in the distributions of the ensemble-averaged velocity and corresponding streamlines. It should be noted that the flow pattern in measurement plane 3 for the FM03 airfoil at AOA = 14.0 deg was found to be quite similar to that of the rigid thin airfoil at the same angle of attack of attack of AOA = 14.0 deg. However, the size of the recirculation bubble in measurement plane 3 behind the FM03 airfoil was found to be smaller than that in the wake of the rigid thin airfoil shown in Fig. 7. The PIV measurements again indicate a smaller aerodynamic drag force acting on the FM03 airfoil than on the rigid thin airfoil, which is confirmed from the measured airfoil drag-coefficient data given in Fig. 4.

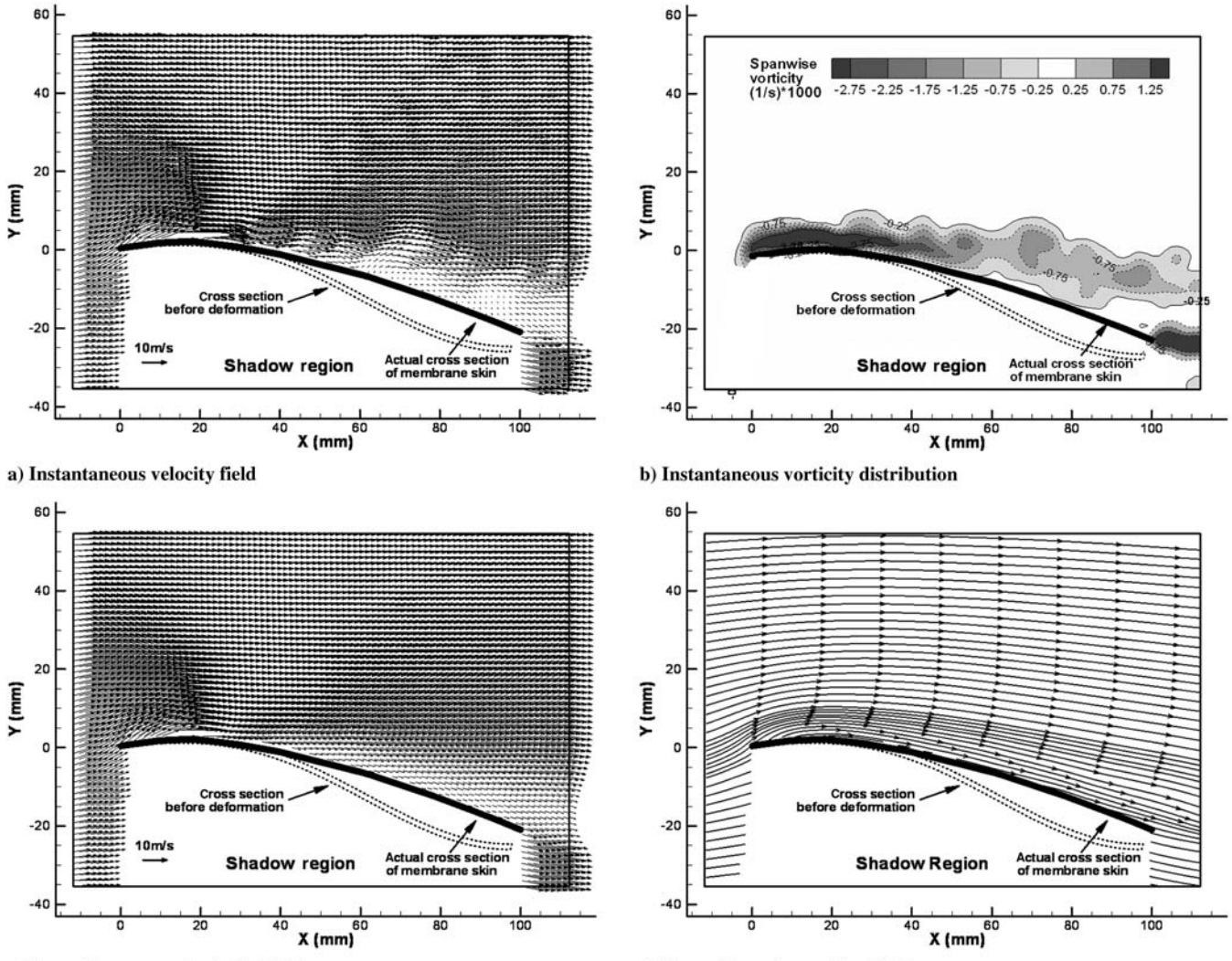

a) Instantaneous velocity field

b) Instantaneous vorticity distribution

c) Ensemble-averaged velocity field

d) Streamlines of mean flowfield

Fig. 9 PIV measurements in measurement plane 1 for the FM03 airfoil at AOA = 14.0 deg.

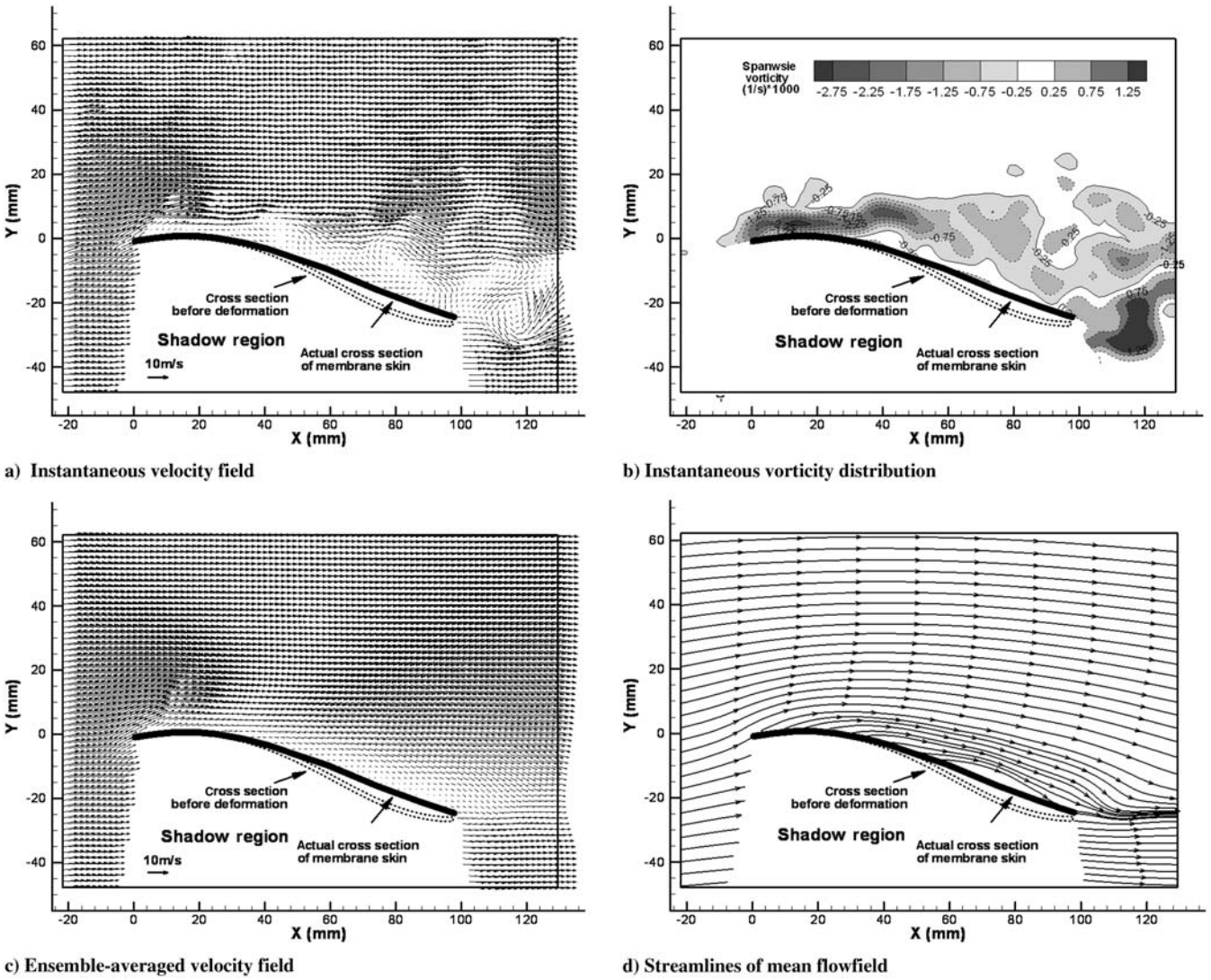

Fig. 10 PIV measurements in measurement plane 2 for the FM03 airfoil at AOA = 14.0 deg.

From the comparison of the PIV measurement results shown in Figs. 9–11, it is evident that the nonuniform spanwise deformation of the flexible-membrane skins for the flexible-membrane airfoils would significantly affect the characteristics of vortex and turbulent flow structures around the flexible-membrane airfoils. Flowfields around the flexible-membrane airfoils were found to become very complicated and fully three-dimensional, even in terms of ensemble-averaged flow quantities. It is conjectured that the spanwise variations of the flow-velocity distributions around the flexible-membrane airfoils would result in the generation of streamwise vortex structures in the wake of the airfoils, which would alter the evolution of trailing vortex structures and modify the induced drag acting on the flexible-membrane airfoils. Further investigation in the future is suggested to elucidate the effects of the nonuniform spanwise deformation of the flexible-membrane skins on the flow features around the flexible-membrane airfoils.

Figure 12 shows the PIV measurement results in measurement plane 1 for the FM03 airfoil at AOA = 18.0 deg. Compared with those cases with smaller angles of attack shown in Figs. 8 and 9, the cross-sectional shape of the FM03 airfoil was found to deform much more dramatically. Airfoil trailing-edge defection (i.e., the lift-up of the airfoil trailing edge from its original position) in measurement plane 1 became more significant due to a more severe pressure difference acting on the upper and lower surfaces of the FM03 airfoil at AOA = 18.0 deg. Incoming flow streams were found to separate from the upper surface of the airfoil in measurement plane 1 eventually, due to the much more significant adverse pressure gradient over the upper surface of the airfoil. Strong, unsteady vortex structures were found to be generated in the flowfield. Large-scale flow separation was found to take place on most portions of the airfoil upper surface. As a result, a fairly large recirculation bubble was found to form in the wake of the FM03 airfoil in the PIV measurement plane 1 at AOA = 18.0 deg. It indicates that the flow around the airfoil was in stall state even in measurement plane 1. A significant increase of the aerodynamic drag force acting on the FM03 airfoil would be expected, which is again confirmed from the aerodynamic force measurement data shown in Fig. 4.

To reveal the deformation of the flexible-membrane skins of the FM03 airfoil more clearly and quantitatively, the actual shapes of the deformed cross section of the FM03 airfoil in measurement plane 1 were extracted from PIV raw images at different angles of attack. The results are given in Fig. 13. The designed profile (i.e., original shape without any deformation) of the airfoil cross section is also given in the figure as the baseline for comparison. It can seen clearly that the cross-sectional shape of the FM03 airfoil deformed more and more significantly with the increasing angle of attack, due to more and more severe stretch to the flexible-membrane skins of the FM03 airfoil. In addition to changing in the geometry shape of the airfoil cross section, airfoil trailing-edge deflection (i.e., the lift-up of the airfoil trailing edge from its original position) was found to become more and more significant as the angle of attack increased. Figure 14 shows the amplitude variations of the airfoil trailing-edge deflection in measurement plane 1 for the FM03 airfoil as a function of the angle

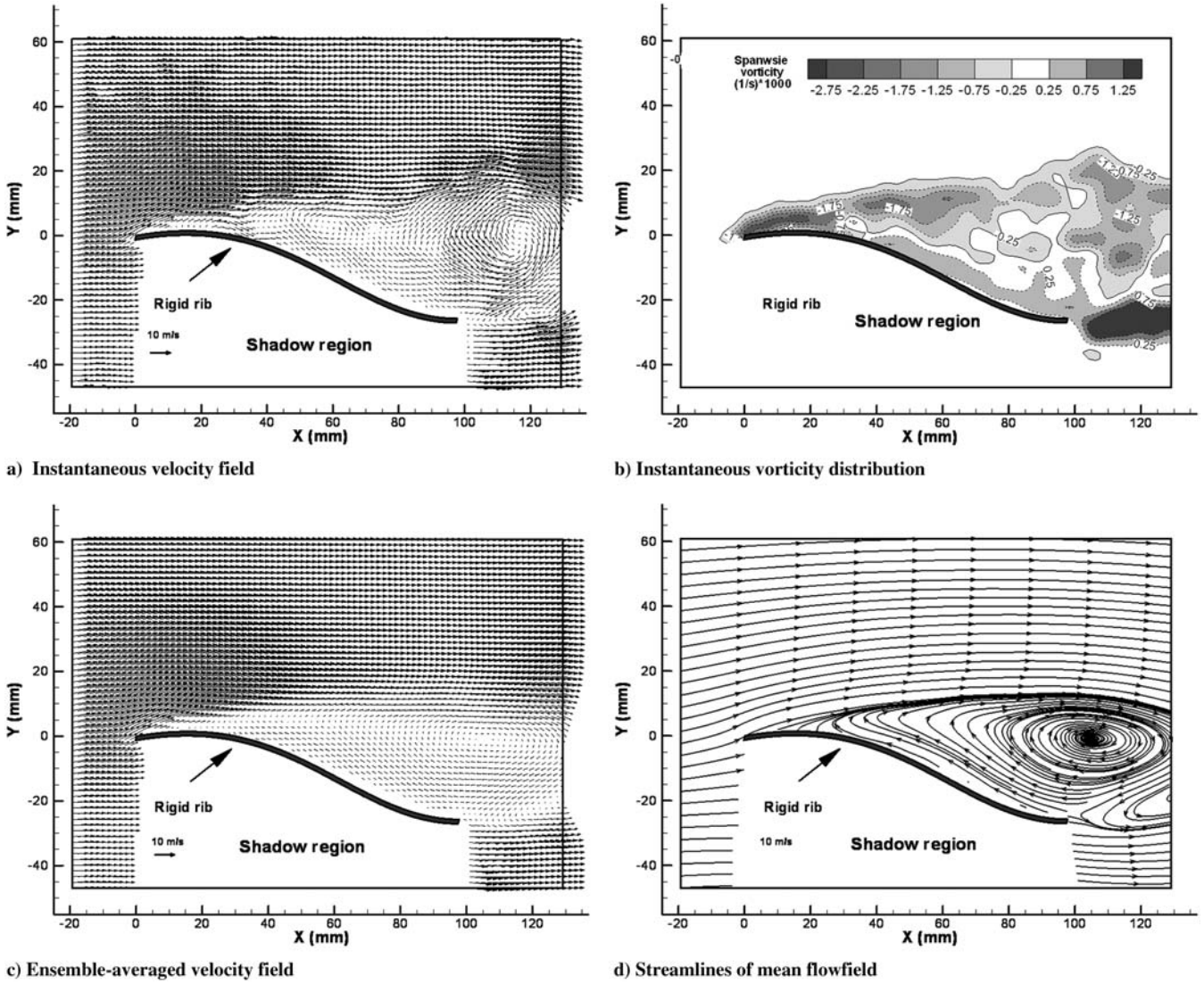

Fig. 11 PIV measurements in measurement plane 3 for the FM03 airfoil at AOA = 14.0 deg.

of attack. It can been seen clearly that the deflection amplitude increased rapidly as the angle of attack of the airfoil increased. The amplitude of the trailing-edge deflection in measurement plane 1 was found to be as high as 6.8% of the chord length for the FM03 airfoil at AOA = 18.0 deg.

Conclusions

An experimental study was conducted to quantify the benefits of using flexible-membrane airfoils/wings at low Reynolds numbers for MAV applications compared with their rigid counterpart. The experiments were conducted in a wind tunnel with the chord Reynolds number of $Re_c = 70,000$. By adding different numbers of rigid ribs to the same membrane-airfoil configuration to adjust the flexibility of the membrane skins of the airfoils, the effects of the flexibility of the membrane airfoils on their aerodynamic performance were assessed in the present study. In addition to measuring aerodynamic forces (lift and drag) acting on the flexible-membrane airfoils/wings, a high-resolution particle image velocimetry (PIV) system was be used to conduct detailed flowfield measurements to visualize the transient behavior of vortex and turbulent flow structures around the flexible-membrane airfoils/wings compared with those around a rigid thin airfoil at different angles of attack. The flowfield measurements were correlated with the aerodynamic force measurements to elucidate the underlying fundamental physics to explore/optimize design paradigms for the development of novel bioinspired flexible-membrane-wing-based MAVs for improved aerodynamic performance.

The aerodynamic force measurement results elucidated clearly that flexible-membrane airfoils/wings could provide better aerodynamic performance than their rigid counterpart. The PIV measurements elucidated that flexible-membrane airfoils could change their camber (i.e., cross-sectional shape) automatically to adapt to incoming flows to balance the pressure differences on the upper and lower surfaces of the airfoils, thereby suppressing large-scale flow separation on the airfoil upper surfaces. Meanwhile, deformations of the flexible-membrane skins were found to cause significant airfoil trailing-edge deflections (i.e., to lift the airfoil trailing edge up from its original designed position), which resulted in reduction of the effective angles of attack of the flexible-membrane airfoils, thereby delaying airfoil stall at high angles of attack.

The PIV measurements also revealed that the nonuniform spanwise deformation of the flexible-membrane skins for the flexible-membrane airfoils significantly affected the characteristics of vortex and turbulent flow structures around the flexible-membrane airfoils. Flowfields around the flexible-membrane airfoils were found to become very complicated and fully three-dimensional, even in terms of ensemble-averaged flow quantities. It is conjectured that the spanwise variations of the flow-velocity distributions around the flexible-membrane airfoils would result in the generation of

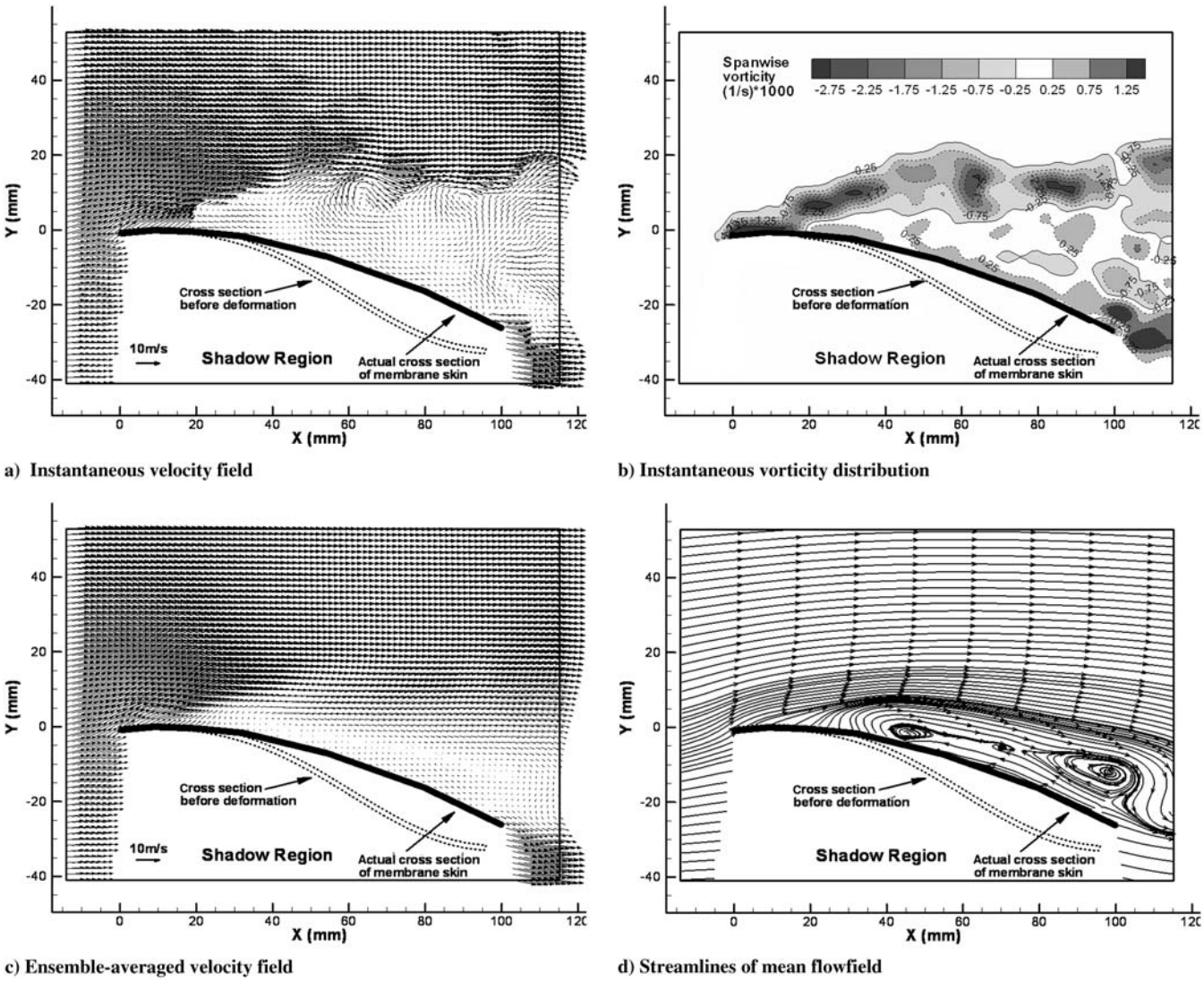

Fig. 12 PIV measurements in measurement plane 1 for the FM03 airfoil at AOA = 18.0 deg.

streamwise vortex structures in the wakes of the airfoils, which would alter the evolution of trailing vortex structures and modify the induced drags acting on the flexible-membrane airfoils.

It is revealed that the flexibility (rigidity) of the membrane skins of the airfoils has a strong effect on their aerodynamic performance. If membranes skins are too flexible, trailing-edge fluttering phenomena may occur, resulting in poor aerodynamic performance at relatively low angles of attack. If membrane skins are too rigid, it would limit the abilities of the flexible-membrane skins to adapt to incoming flows to suppress large-scale flow separation and delay airfoil stall, thereby degrading the aerodynamic performance of the airfoils at relatively high angles of attack.

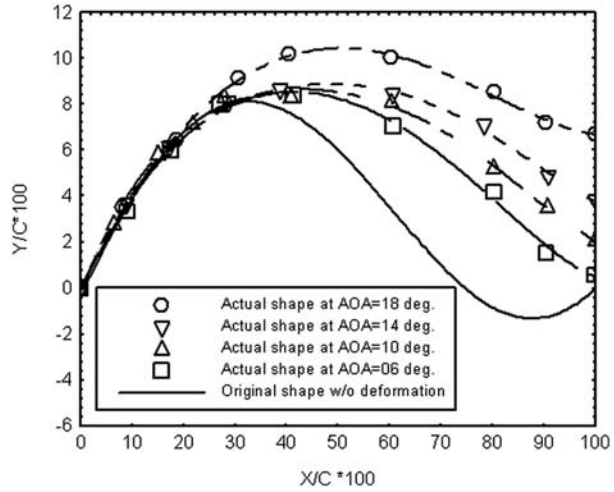

Fig. 13 The actual cross-sectional shapes of the FM03 airfoil in measurement plane 1 at different angles of attack.

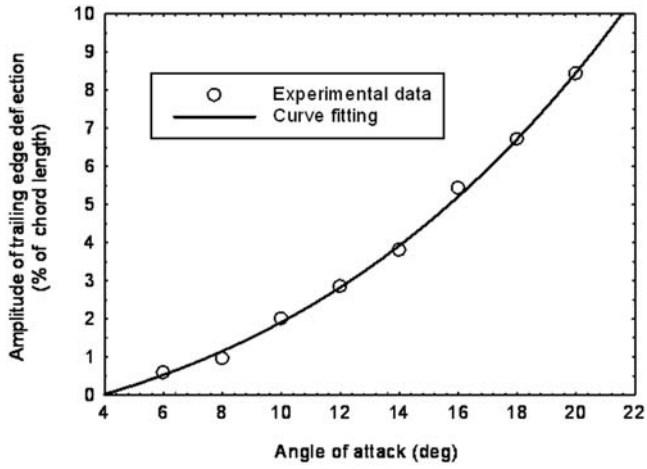

Fig. 14 Amplitude of the airfoil trailing-edge deflection of the FM03 airfoil in measurement plane 1 vs the angle of attack.

Acknowledgment

The support of National Science Foundation CAREER program under award number CTS-0545918 is gratefully acknowledged.

References

[1] Carmichael, B. H., "Low Reynolds number airfoil Survey," Vol. 1, NASA CR-165803, 1981.

[2] Lissaman, P. B. S., "Low-Reynolds-Number Airfoils," *Annual Review of Fluid Mechanics*, Vol. 15, 1983, pp. 223–239. doi:10.1146/annurev.fl.15.010183.001255

[3] Gad-el-Hak, M., "Micro-Air-Vehicles: Can They be Controlled Better," *Journal of Aircraft*, Vol. 38, No. 3, 2001, pp. 419–429.

[4] Mueller T. J. (ed.), *Fixed and Flapping Wing Aerodynamics for Micro Air Vehicle Applications*, Progress in Astronautics and Aeronautics, AIAA, Reston, VA, 2001.

[5] Galvao, R., Israeli, E., Song, A., Tian, X., Bishop, K., Swartz, S., and Breuer, K., "The Aerodynamics of Compliant Membrane Wings Modeled on Mammalian Flight Mechanics," AIAA Paper 2006-2866, 2006.

[6] Weinstein, R., Hueso, E., Pivkin, I., Swartz, S., Laidlaw, D. H., Karniadakis, G., and Breuer, K. S., "Simulation and Visualization of Flow Around Bat Wings During Flight," *SIGGRAPH 2004* [CD-ROM], ACM Press, New York, 2004.

[7] Swartz, S., Diaz, J., Riskin, D. K., Song, A., Tian, X., Willis, D. J., and Breuer, K. S., "Wing Structure and the Aerodynamic Basis of Flight in Bats," AIAA Paper 2007-0042, 2007.

[8] Song, A., and Breuer, K., "Dynamics of a Compliant Membrane as Related to Mammalian Flight," AIAA Paper 2007-665, 2007.

[9] Ifju, P. G., Ettinger, S., Jenkins, D. A., and Martinez, L., "Composite Materials for Micro Air Vehicles," *SAMPE Journal*, Vol. 37, No. 4, 2001, pp. 7–13.

[10] Albertani, R., Boria, F., Bowman, S., Claxton, D., Crespo, A., Francis, C., Ifju, P., Johnson, B., Lee, H. K., Morton, M., and Sytsma, M., "Development of Reliable and Mission Capable Micro-Air-Vehicles," *9th International MAV Competition*, 2005, pp. 1–10.

[11] Shyy, W., Ifju, P., and Viieru, D., "Membrane Wing-Based Micro Air Vehicles," *Applied Mechanics Reviews*, Vol. 58, No. 4, 2005, pp. 283–301. doi:10.1115/1.1946067

[12] Albertani, R., Stanford, B., Hubner, J. P., and Ifju, P. G., "Aerodynamic Coefficients and Deformation Measurements on Flexible Micro Air Vehicle Wings," *Experimental Mechanics*, Vol. 47, No. 5, 2007, pp. 625–635. doi:10.1007/s11340-006-9025-5

[13] Abdulrahim, M., "Dynamic Characteristics of Morphing Micro Air Vehicles," M.S., Thesis, Dept. of Mechanical and Aerospace Engineering, Univ. of Florida, Gainesville, FL, 2004.

[14] Smith, R. W., and Shyy, W., "Computation of Unsteady Laminar Flow Over a Flexible Two-Dimensional Membrane Wing," *Physics of Fluids*, Vol. 7, No. 9, 1995, pp. 2175–2184. doi:10.1063/1.868467

[15] Shyy, W., Berg, M., and Ljunqvist, D., "Flapping and Flexible Wings for Biological and Micro Air Vehicles," *Progress in Aerospace Sciences*, Vol. 35, No. 5, 1999, pp. 455–506. doi:10.1016/S0376-0421(98)00016-5

[16] Shyy, W., Jenkins, D. A., and Smith, R. W., "Study of Adaptive Shape Airfoils at Low Reynolds Number in Oscillatory Flows," *AIAA Journal*, Vol. 35, No. 9, 1997, pp. 1545–1548.

[17] Tang, J., Viieru, D., and Shyy, W., "A Study of Aerodynamics of Low Reynolds Number Flexible Airfoils," AIAA Paper 2007-4212, 2007.

[18] Waszak, R. M., Jenkins, N. L., and Ifju, P., "Stability and Control Properties of an Aeroelastic Fixed Wing Micro Aerial Vehicle," AIAA Paper 2001-4005, 2001.

[19] Warkentin, J., and DeLaurier, J., "Experimental Aerodynamic Study of Tandem Flapping Membrane Wings," *Journal of Aircraft*, Vol. 44, No. 5, 2007, pp. 1653–1661. doi:10.2514/1.28160

[20] Null, W., and Shkarayev, S., "Effect of Camber on the Aerodynamics of Adaptive-Wing Micro Air Vehicles," *Journal of Aircraft*, Vol. 42, No. 6, 2005, pp. 1537–1642. doi:10.2514/1.12401

[21] Tamai, M., "Experimental Investigations on Biologically Inspired Airfoils for MAV Applications," M.S. Thesis, Aerospace Engineering Dept., Iowa State Univ., Ames, IA, 2007.

[22] Lian, Y., and Shyy, W., "Three-Dimensional Fluid-Structure Interactions of a Membrane Wing for Micro Air Vehicle Applications," *Journal of Aircraft*, Vol. 42, No. 4, 2005, pp. 865–873. doi:10.2514/1.5909